Surface-enhanced Raman spectroscopy biosensors: excitation spectroscopy for optimisation of substrates fabricated by nanosphere lithography

X. Zhang, C.R. Yonzon, M.A. Young, D.A. Stuart and R.P. Van Duyne

Abstract: In the 28 years since its discovery, surface-enhanced Raman scattering (SERS) has progressed from model system studies of pyridine on a roughened silver electrode to state-of-the-art surface science studies and real-world sensing applications. Each year, the number of SERS publications increases as nanoscale material design techniques advance and the importance of trace analyte detection increases. To achieve the lowest limits of detection, both the relationship between surface nanostructure and laser excitation wavelength and the analyte–surface binding chemistry must be carefully optimised. This work exploits the highly tunable nature of nanoparticle optical properties to establish the optimisation conditions. Two methods are used to study the optimised conditions of the SERS substrate: plasmon-sampled and wavelength-scanned surfaced Raman excitation spectroscopy (SERES). The SERS enhancement condition is optimised when the energy of the localised surface plasmon resonance of the nanostructures lies between the energy of the excitation wavelength and the energy of the vibration band of interest. These optimised conditions enabled the development of SERS-based sensors for the detection of a *Bacillus anthracis* biomarker and glucose in a serum–protein matrix.

1 Introduction

Inelastic photon scattering was first witnessed by C.V. Raman and K.S. Krishnan in 1928 [1], a process later to bear the name Raman scattering and to garner its discoverer a Nobel Prize in 1930. Raman scattering is a very inefficient process, in that approximately one photon is inelastically scattered for every 10^{10} elastically scattered photons. In a simple classical view of the Raman effect, incident light is considered as an electromagnetic wave that induces polarisation in a molecule. Then, the induced dipole emits or scatters light at the optical frequency of the incident light wave, plus or minus the energy of a molecular vibration. The magnitude of the induced polarisation, P, is related to the molecular polarisability, α, and the magnitude of the incident electric field, E, by [2]:

$$P = \alpha E \tag{1}$$

The molecular polarisability describes the ease with which the electron cloud around a molecule can be distorted by the electric field. The strength of E is dependent on the power and wavelength of the incident electromagnetic field. In surface-enhanced Raman scattering (SERS), the E field is increased by a factor of 10–1000 by the nanoscale optical properties of the enhancing substrate, as described below.

Several technological developments, such as laser light sources for excitation, holographic notch filters and gratings, and array-based detectors, led to a renaissance in Raman spectroscopy. Raman spectroscopy finds increasing application in materials characterisation, biochemistry and even art conservation, owing to the rich spectral information and the ability to obtain spectra for non-transparent solids or aqueous samples. The advent of micro-Raman techniques permits characterisation of small quantities of materials with high spatial resolutions [2]. Recently, the combination of laser trapping [3, 4] with Raman microscopy has enabled the spatially localised study of chemical species and reactions in single micrometre-sized [5] or even nanometre-sized volumes [6]. Raman spectroscopy is no longer an under-utilised, but information-rich, spectroscopic technique; rather, it is a powerful tool for the fundamental study of molecular structure, dynamics and analysis.

As the Raman effect is inherently weak, it is usually difficult to use normal Raman scattering either for trace analysis or for the study of highly fluorescent samples [2]. One way to overcome this problem is to use surface-enhanced Raman spectroscopy. SERS is a plasmonic phenomenon whereby molecules at or near a noble metal surface with nanoscale structural features experience a dramatic increase in the incident electromagnetic field, yielding high Raman intensity. SERS can increase the Raman intensity of a molecule in proximity to a nanoscale roughened surface by 10^8 [7, 8], and up to 10^{14} times under special circumstances [9, 10]. The mechanism responsible for this large enhancement in Raman intensity continues to be the subject of considerable research [11–16]. However, it is generally agreed that two mechanisms contribute to the overall enhancement: a chemical effect (CHEM) and an electromagnetic enhancement (EM).

The theory of chemical enhancement was invoked to account for the discrepancy between the enhancements predicted in the initial electromagnetic models ($\sim 10^4$) and the empirically determined enhancement ($\sim 10^6$). It is thought that 'active sites', either crystal defects or adatoms on the surface of the metal, undergo a charge-transfer process enabling the CHEM enhancement. The dependence

IEE Proceedings online no. 20050009

doi:10.1049/ip-nbt:20050009

Paper first received 17th May and in final revised form 4th November 2005

The authors are with the Department of Chemistry, Northwestern University, Evanston, IL 60201, USA

Email: vanduyne@chem.northwestern.edu

of the optimum SERS excitation frequency on electrode potential suggests that new electronic states may arise upon adsorption of the analyte, which leads to resonant intermediate states for Raman scattering [17]. The CHEM enhancement has been investigated, particularly the effect of halide ions on increasing SERS [16, 18]. However, because the chemical environment of a given sample may be largely outside experimental control (e.g. in biological media), or determined by other factors (e.g. in ultra high vacuum systems), it is often difficult to exploit the CHEM enhancement mechanism. Furthermore, because electromagnetic enhancement is the dominant contributor to SERS, and because of the large variety of substrate materials and geometries available, maximising the electromagnetic enhancement provides the most convenient and effective handle to optimise SERS in a typical empirical setting. Modern advances in both experimental science and theoretical modelling allow better understanding of, and control over, SERS than ever before.

The discovery of single-molecule SERS (SMSERS) by Emory and Nie [9] and Kneipp *et al.* [10], in 1997, has necessitated a re-examination of the EM mechanism. The EM mechanism is based on the significantly amplified electromagnetic fields (E) generated by the localised surface plasmon resonance (LSPR) of nanoscale surface roughness features [12]. It is the intricate relationship between the surface structure and the structurally dependent optical characteristics that determines the magnitude of the EM portion of SERS enhancement [7, 8]. In the so-called 'lightning rod effect', nanoscale features such as sharp points or interparticle junctions can generate intense EM fields that can amplify both the incoming excitation photons and the exiting Stokes shifted photons by orders of magnitude [12, 19, 20]. These factors must be well-controlled for SERS to be used effectively [21].

The EM mechanism has several experimental signatures, such as long-range (i.e. a few nanometres) distance dependence [22–24], the weak dependence of the enchantment factor (EF) on the chemical identity of the adsorbate [25] and the existence of surface-enhanced second harmonic generation (SESHG) [26–28] SMSERS. The improved understanding of the nature of the EM enhancements has generated renewed interest in the use of SERS as an analytical technique. Many groups continue to generate new insights as new mathematical models are coupled to more accurate characterisation in the nanoscale regime [29, 30].

SERS possesses many desirable characteristics as a tool for the chemical analysis of interfacial molecular species, including high specificity attomole to high zeptomole mass sensitivity [9, 10], micromolar to picomolar concentration sensitivity [21] and interfacial generality [31, 32]. Other examples include concentration-jump or potential step studies of adsorption/desorption kinetics at electrode or colloid surfaces [33] and the use of ultra fast, pulsed laser excitation to probe vibrational relaxation, energy transfer or electron dynamics at surfaces [34, 35]. Recently, SERS has been used in the quantitative detection and analysis of bio-related molecules [21, 36–38]. The variation in surface enhancement is easily corrected for by addition of an internal standard to the samples [21]. Ideally, the signal intensities from the internal standard should be comparable with those of the analyte, and one or more bands should be in spectrally silent regions. Internal standards with only a few spectral bands are preferable for easier data evaluation. However, in many instances, the addition of internal standards is either impossible, or would unduly interfere with the analyte or process under observation. Therefore it is desirable to be able to produce SERS substrates that not only provide the optimum EF, but also are stable from substrate to substrate and from experiment to experiment.

The first SERS experiments generated largely random structures, and enhancement factors could vary wildly. Modern synthetic techniques allow exquisitely precise control over nanoscale features and thus over the nanoscale optical properties upon which SERS intimately depends. The choice of substrates with specific, well-defined and controlled LSPR and laser excitation wavelength, λ_{ex}, is the critical factor that affects the resulting SERS EF and, accordingly, the analytical limit of detection (LOD). This review will demonstrate how the SERS enhancement factor depends on these characteristics.

The remainder of this review will be organised into three parts. First, we compare the available methods for fabrication of SERS-active surfaces. Secondly, we discuss techniques designed to optimise the EM enhancement [7, 8]. Specifically, we describe both wavelength-scanned and plasmon-sampled SERS excitation spectroscopy. Thirdly, we review the most recent progress in the SERS-based sensors for two important target molecules: a *Bacillus anthracis* biomarker [21, 39] and glucose in a serum protein mixture [36, 38].

2 SERS-active surfaces

SERS is usually performed on Ag [13], Au [40] or Cu [41] surfaces, because these metals have appropriate values of the real and imaginary parts of the dielectric constant [42] and can be easily handled in ambient, electrochemical and ultra-high vacuum environments. With the variety of SERS-active surfaces available today, e.g. colloids, colloid in sol-gel [43], electrochemically roughened electrodes [11, 13], vapour-deposited metal island films [44] and lithography-produced nanostructures [45], researchers are able to select the SERS substrate architecture that best matches their experimental needs.

The preparation of noble metal colloids has been studied since ancient times [46]. Colloidal substrates can be prepared in many different shapes [47, 48], such as spheres, rod-shaped [49, 50], cubes, triangles [51, 52] and shells [53, 54]; they can be dispersed throughout the object of study and even inside macrostructures [55], such as cells [56] and tissue samples [57]. However, the distribution of shapes and sizes and the ease of aggregation will influence the surface-enhancing properties.

The nanoparticle synthesis methods discussed above create suspensions of nanoparticles in solution. Another class of fabrication techniques yields surface-bound nanostructures. The standard approach for making surface-bound nanostructures is electron beam lithography (EBL). In EBL, the desired pattern is serially produced by the exposure of a thin layer of photo resist to high-energy electrons, followed by chemical development and deposition of the noble metal. Several research groups have focused on the optical properties of two-dimensional arrays to utilise these nanoparticle assemblies as surface-enhanced spectroscopy substrates [30, 58, 59]. Although EBL provides exquisite control over interparticle spacing and can fabricate arbitrary shapes, it is an expensive and slow, serial form of lithography.

An alternative method for the large-scale production of surface-bound nanoparticle arrays is nanosphere lithography (NSL). NSL is a powerful fabrication technique that inexpensively produces nanoparticle arrays with controlled shape, size and interparticle spacing [60]. Every NSL structure begins with the self-assembly of size-monodisperse

nanospheres of a uniform diameter, D, to form a two-dimensional colloidal crystal deposition mask [60–63]. As the solvent evaporates, capillary forces draw the nanospheres together, and the nanospheres crystallise in a hexagonally close-packed pattern on the substrate (Fig. 1). As in all naturally occurring crystals, nanosphere masks include a variety of defects that arise as a result of nanosphere polydispersity, site randomness, point defects, line defects and polycrystalline domains. Typical defect-free domain sizes are in the 10–100 μm range. Following self-assembly of the nanosphere mask, a metal or other material is then deposited by thermal evaporation, electron beam deposition or pulsed laser deposition to a target metal thickness, d_m. After metal deposition, the nanosphere mask is removed, leaving behind surface-confined nanoparticles with triangular footprints (Fig. 1*a*). At mass thicknesses exceeding 100 nm, a continuous film of metal is deposited on the nanospheres (Fig. 1*b*). These metal film over nanosphere (MFON) substrates are some of the most robust SERS substrates available in terms of spectral stability, sample-to-sample uniformity and mechanical ruggedness [45]. The diameter of the nanosphere cores and the thickness of the metal film shell determine the size distribution of the roughness features and, hence, the optical response. Even though the nanoscale roughness features are not homogeneous in size but, instead, are driven by the larger-scale templating, they are sufficiently uniform to generate a relatively narrow surface plasmon peak (FWHM ~200 nm) [21]. Recent experiments have conclusively demonstrated that MFON substrates are stable for months [21] (unlike many other nanostructured surfaces) and remain SERS-active even when exposed to large temperature [64] and electrochemical potential excursions [39].

3 Optimisation of SERS by surface-enhanced Raman excitation spectroscopy

3.1 Plasmon-scanned surface-enhanced Raman excitation spectroscopy

Plasmon-sampled surface-enhanced Raman excitation spectroscopy (PS SERES) was developed to explore the relationship between nanoparticle optics and the resulting EF [65]. In the PS SERES experiment, a Raman-active molecule is adsorbed onto the substrate of choice, and then the correlated SERS and LSPR spectra of that adsorbate are captured from a microscale domain using a single laser excitation wavelength. This procedure can be repeated on a single substrate until all the different LSPR domains have been sampled. The use of NSL fabricated arrays permits agile frequency tuning of the LSPR based on the nanosphere mask dimensions, metal thickness and metal type. The intensity or enhancement factor of a specific Raman band is plotted against the LSPR maximum to reveal the optimised experimental conditions. There are multiple advantages in performing the PS SERES profiling:

(*a*) the number of data points in the PS SERES profile is only limited by the number of microscale sample regions (and fabricated substrates) with different LSPR characteristics

(*b*) the experiment requires only a single laser excitation wavelength, a single notch filter and a single stage monochromator

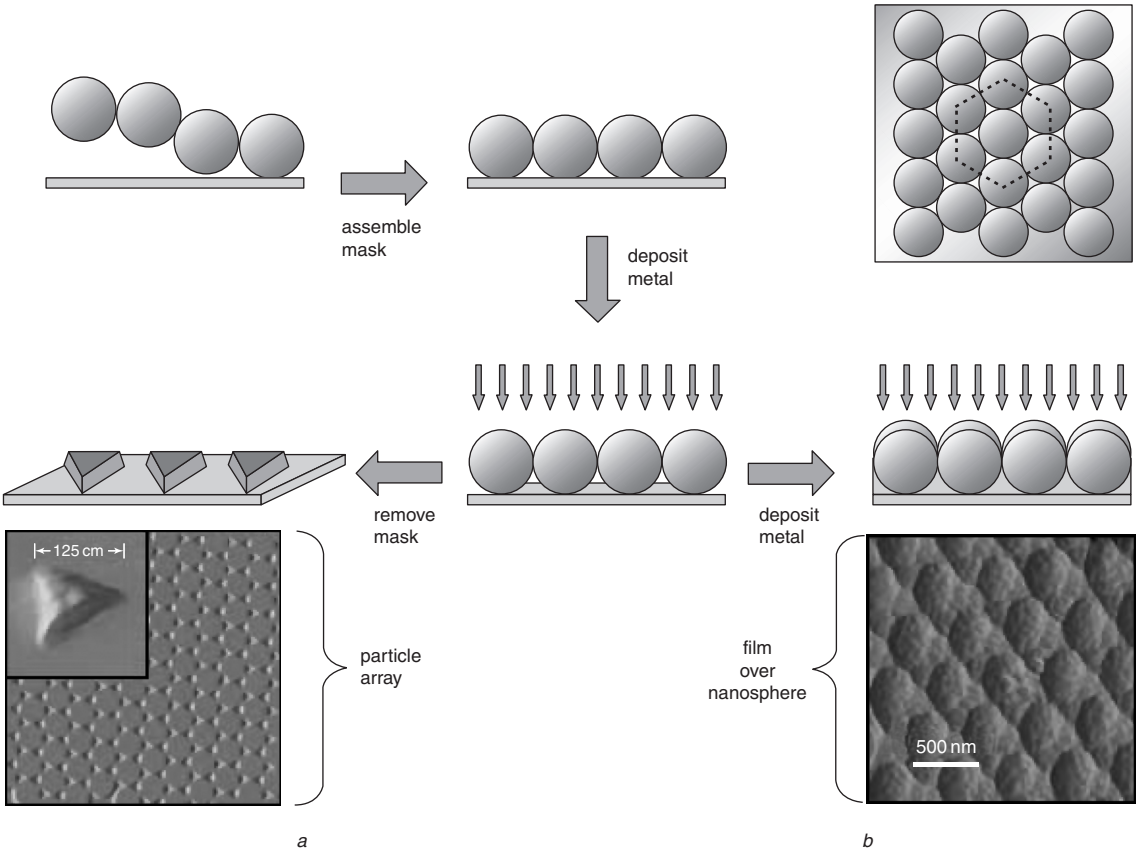

Fig. 1 *Nanosphere lithographic fabrication of triangular particle array and metal film over nanosphere (MFON) substrates*
Carboxylate modified polymer microspheres of uniform diameter are self-assembled into hexagonally close-packed array on supporting substrate. Metal (typically Ag or Au) is deposited through sphere array, which serves as deposition shadow mask
a Array of triangular-shaped particles is formed in interstices between spheres, which can be removed by sonication
b If >100 nm of metal is deposited, continuous film covers spheres, forming FON surface

(*c*) the information gained gives the general guidelines for achieving an optimised EF on any substrate with a narrow LSPR.

NSL-fabricated Ag nanotriangles were used as SERS substrates for the PS SERES experiments. The size/shape of these Ag nanotriangles can be tuned systematically by changing the nanosphere size in the deposition mask or the deposition thickness [66, 67]. Slight variations in the size or shape of these nanoparticles yield significant shifts in the narrow LSPR spectrum.

Even though the structural variations among the nanoparticles on a given NSL sample are small, they generate varying LSPR properties between microscale domains. Although it is possible to eliminate much of this variation if necessary, the PS SERES experiment exploits the distribution of optical properties to maximise the number of data points in the excitation profile. In all cases to date, PS SERES experiments have explored adsorbates that bind irreversibly to the silver nanoparticles to simplify data collection and interpretation.

Below we present three separate PS SERES profiles that were constructed using benzenethiol adsorbed onto Ag nanoparticles. Each profile was measured with a different laser excitation wavelength (514.5, 532.0 or 632.8 nm). The correlated LSPR and SERS spectra for the optimised enhancement factor in each case are shown in Fig. 2, and the PS SERES profiles are shown in Fig. 3. The profiles clearly demonstrate that the maximum enhancement factor occurs when the LSPR λ_{max} lies between the energy of the excitation wavelength (solid lines) and the vibration mode (broken lines). It is interesting to note that the enhancement factor does not vary by more than a factor of 10 once the signal is measurable above background.

To ensure that the results observed are not an artifact of the molecule adsorbed on the surface, more PS SERES profiles were constructed with varied molecular adsorbates (3,4-dichlorobenzenethiol, 1,4-benzenedithiol, and $Fe(bpy)_3^{2+}$), and similar results were achieved in all cases. The two non-resonant molecules yielded maximised enhancement factors of 2.3×10^7 and 1.4×10^8, and the maximum enhancement factor for the resonant molecule $Fe(bpy)_3^{2+}$ was 7.1×10^9. To verify that various vibration modes adhere to the demonstrated pattern, PS SERES profiles were constructed for five different vibration modes of 3,4-dichlorobenzenethiol, including in-plane ring deformations, a ring-breathing mode, the C-S stretch and the C-Cl stretch. Again, the maximised enhancement factors occurred when the LSPR λ_{max} was between the excitation wavelength and the wavelength of the vibration mode.

Thus, for practical application, the PS SERES technique has revealed a general rule for optimising EF when substrates with narrow LSPR spectra and a single laser excitation source are used. The largest EF is achieved when the energy corresponding to the narrow LSPR λ_{max} falls within a $\sim$120 nm window that includes the energy of the excitation wavelength and that of the Raman-shifted scattered photons. The LSPR variation on the NSL substrates used in the work presented above can be easily exploited to find the microscale domains with the best optical properties for a given experiment, thus maximising the enhancement factor and lowering the detection limit. Although the reported enhancement factors from NSL microdomains are significantly smaller than those measured in single-molecule SERS studies, these ensemble-averaged values can be regularly achieved, are temporally stable and are more readily understood.

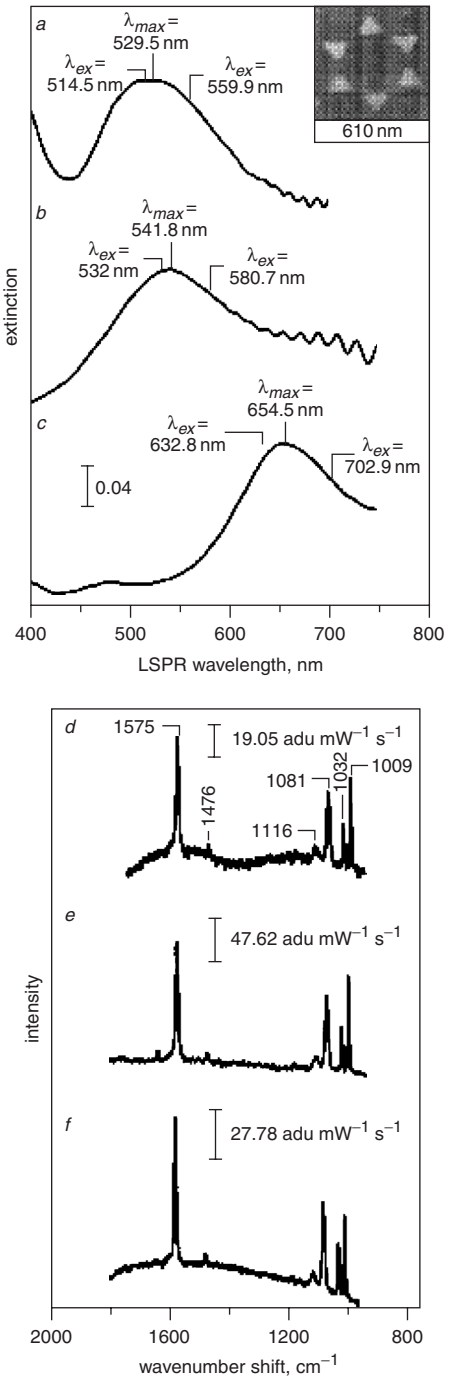

Fig. 2 *Correlated, spatially resolved LSPR extinction and SERS spectra of benzenethiol-dosed NSL substrates with maximised enhancement factors*
a and *d* Measured from $D = 280$ nm, mass thickness of Ag film $d_m = 36$ nm, $P_{ex} = 0.7$ mW, $\lambda_{ex} = 514.5$ nm
b and *e* Measured from $D = 280$ nm, $d_m = 36$ nm, $P_{ex} = 0.7$ mW, $\lambda_{ex} = 532.0$ nm
c and *f* Measured from $D = 400$ nm, $d_m = 56$ nm, $P_{ex} = 0.7$ mW, $\lambda_{ex} = 632.8$ nm
All Raman spectra were captured with integration time of 30 s.
Reproduced with permission from [7]

3.2 Wavelength-scanned surface-enhanced Raman excitation spectroscopy

For all SERS sensing applications, sensitivity is of primary importance. To this end, we have undertaken a study of the fundamental mechanism of SERS to ascertain the specific conditions necessary for maximising the enhancement of the

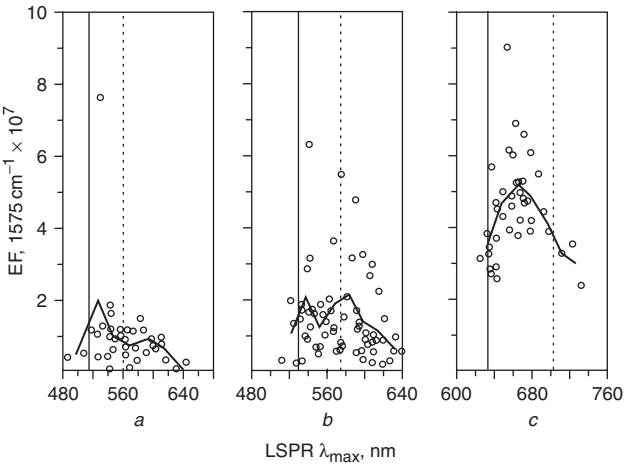

Fig. 3 *PS SERES for ν_{8a} (1575 cm^{-1}) band of benzenethiol with three different excitation wavelengths*
a $\lambda_{ex} = 514.5$ nm
b $\lambda_{ex} = 532.0$ nm
c $\lambda_{ex} = 632.8$ nm
--------- Wavelength location of excitation
- - - - - - - - Wavelength location of scattering
Overlaid line represents bin-averaged values of LSPR λ_{max} and EF

Raman scattering. There are three principle factors that determine the sensitivity of a Raman experiment:

(*i*) the frequency to the fourth (ν^4) scattering dependence of Raman photons

(*ii*) the wavelength-dependent efficiency of the detection system

(*iii*) the relationship between the LSPR of the substrate and the maximum SERS enhancement.

The first factor would indicate that shorter excitation wavelengths are always best, but that is not necessarily the case. For example, in many biological applications, it is often desirable to use near IR excitation to avoid damaging the sample or exciting sample autofluorescence, even at the cost of some signal loss due to ν^4. The second factor is straightforward and is simply a function of the configuration of the spectrograph and detector. Consultation of the efficiency curves of the dispersive elements and the detector are readily available from manufacturers and should factor into purchase planning and experimental design. For example, most systems are configured with gratings and detectors optimised in the visible region of the spectrum, decreasing their efficacy in the UV or NIR region. The third factor, the relationship between the LSPR of the substrate and the maximum SERS enhancement, is more complex and interesting, yet less well understood or utilised. We have explored this third factor using a technique called wavelength-scanned surface-enhanced Raman excitation spectroscopy (WS SERES).

WS SERES involves the measurement of SERS enhancement for several laser excitation wavelengths, λ_{ex}. This technique was recognised as a useful tool for exploring the EM mechanism soon after the discovery of SERS. An obvious limitation of this technique is that the number of data points is determined by the tuneability of the excitation laser and detection system. These substantial instrumental requirements have led to the majority of SERES publications suffering from low data point density and/or limited spectral coverage [31, 68–70]. These limitations prevent the establishment of conclusive generalisations from SERES data. Additionally, most SERES experiments have been performed using surface-enhancing substrates with an unknown or poorly characterised distribution of roughness features. In the few cases where the surfaces are carefully characterised, it has been shown that there is a wide distribution of roughness feature sizes [31, 71]. Other studies do not include characterisation of the LSPR of the substrate [69, 70], which prevents any direct comparison of the excitation profiles with the spectral location of the wavelength of maximum LSPR extinction, λ_{max}.

The most common substrates historically employed in SERES experiments are Ag island films and Ag colloidal solutions. In these cases, most of the SERS excitation profiles peak at excitation wavelengths ($\lambda_{ex,max}$) near 500–600 nm [71–75]. The peaks of the excitation profiles have been shown to shift to longer wavelengths with increased aggregation [68, 71, 73, 74], which is a qualitative result predicted by the EM mechanism. With these types of substrate, it is difficult to make a direct comparison between the LSPR of the substrate and the SERS excitation profile, because the LSPR of the substrate is a superposition of a wide variety of LSPR wavelengths corresponding to the different roughness features caused by morphological (size and shape) polydispersity between islands or colloidal nanoparticles.

Two exceptions to the above statements regarding roughness features are the well-known experiments by Liao and co-workers on microlithographically prepared Ag posts [76] and recent work by Felidj and co-workers on EBL-produced arrays of gold elongated nanoparticles [77]. The former ground-breaking work demonstrated excitation profiles where $\lambda_{ex,max}$ shifted to longer wavelengths with increased particle aspect ratio and with increased dielectric constant of the medium surrounding the particles. These results qualitatively agree with the EM mechanism, but the LSPR of these substrates was not measured for a direct comparison. In the latter work, the SERS enhancement was shown to peak halfway between the excitation wavelength and the wavelength of the Raman scattered photon. This important experiment was the first observation of precisely what is predicted by the EM mechanism. Unfortunately, this result was only obtained on one sample with a profile consisting of only three data points.

Herein, we describe the utilisation of a broadly tuneable Raman system to measure excitation profiles with the greatest number of data points ever achieved in a WS SERES experiment. A broadly tuneable laser system, a versatile detection system and a well-characterised surface-enhancing substrate are all employed to surmount the traditional shortcomings of WS SERES experiments. The use of a CW mode-locked Ti : sapphire and its harmonics allows for continuous tuneability over the spectral ranges 350–500 nm and 700–1000 nm. The visible region not covered by the Ti : sapphire system was augmented with the use of a solid-state laser and a tuneable dye laser. A triple spectrograph equipped with a CCD camera allows for rapid, multichannel spectral acquisition with efficient rejection of Rayleigh-scattered photons. The SERS substrates used in this work are triangular nanoparticle arrays fabricated by NSL. These substrates have been well characterised previously [61, 66, 67]. They present a significant advantage over many of the traditional SERS substrates for SERES studies, because NSL-fabricated triangular nanoparticles exhibit extremely narrow size distributions, making them an indispensable tool for probing the fundamental characteristics of SERS. Tuneability of the LSPR λ_{max} of these nanoparticles throughout the visible and NIR wavelengths can be achieved by systematic variation of the dimension of the nanoparticles [66]. Even though the surface coverage of these nanoparticles is

~7%, strong SERS intensities are observed from analytes adsorbed to these substrates, owing to the strong enhancement NSL-fabricated arrays exhibit [65].

For the work presented below, the intensity of the 1575 cm^{-1} band of a benzenethiol monolayer adsorbed to the Ag nanoparticles was measured at many different excitation wavelengths, λ_{ex}. Benzenethiol is used as a model molecule in both this and the following sections because it:

(*a*) binds *via* the thiol group to the metal surface

(*b*) has a high Raman scattering cross-section

(*c*) lacks electronic transitions in the visible range, rendering it non-resonant at the excitation wavelengths used

(*d*) has a well-resolved spectrum.

To account for any variation of the SERS intensity not due to the enhancement by the substrate, the 1444 cm^{-1} normal Raman scattering band of neat cyclohexane was used as an intensity standard. This standard was used to correct for the inherent ν^4 behaviour of Raman scattering, spectral dependence of the detection system and differences in the illumination power.

Figure 4 shows four excitation spectra for the 1575 cm^{-1} peak of benzenethiol, each with an LSPR λ_{max} at a distinctly different location. The SERES spectrum in Fig. 4*a* is measured over the spectral range 420–500 nm. Because the formation of a monolayer of benzenethiol on these nanoparticle arrays results in a large red shift in the position of the LSPR λ_{max}, it was necessary to anneal this sample at 300°C for 1 h prior to benzenethiol addition, to achieve a final LSPR λ_{max} at a wavelength shorter than 500 nm. It has been previously shown that annealing NSL-derived samples results in a large blue shift of the LSPR owing to the shape of the nanoparticles being changed [66]. The LSPR λ_{max} of this substrate was measured to be 489 nm (20 450 cm^{-1}). The largest SERS enhancement occurs at $\lambda_{ex} = 485$ nm. Fitting a Gaussian line shape to the data reveals that the peak of the excitation profile, $\lambda_{ex,max}$, is 480 nm (20 833 cm^{-1}). The peak enhancement factor (EF) value for this sample was calculated to be 5.5×10^5. This value is low in comparison with the values determined for the other samples, because the shape of the nanoparticles is made more ellipsoidal by annealing. In addition to shifting the LSPR λ_{max} to shorter wavelengths, this change decreases the intensity of the electromagnetic fields at the nanoparticle surfaces by removing the sharp corners that are calculated to possess the greatest field enhancements [12].

The SERES spectrum in Fig. 4*b* was measured over the spectral range 532–690 nm. The LSPR λ_{max} of this substrate was measured to be 663 nm (15 083 cm^{-1}). The largest SERS enhancement occurs for $\lambda_{ex} = 625$ nm. The maximum of a Gaussian line shape fit to the data is 625 nm (16 000 cm^{-1}). The peak EF value for this sample is 1.2×10^7. The SERES spectrum in Fig. 4*c* is measured over the spectral range 532–740 nm. The LSPR λ_{max} of this substrate was measured to be 699 nm (14 306 cm^{-1}). The largest SERS enhancement occurs for $\lambda_{ex} = 670$ nm. The maximum of a Gaussian line shape fit to the data is 671 nm (14 903 cm^{-1}). The peak EF value for this sample is 1.4×10^7. The SERES spectrum in Fig. 4*d* is measured over the spectral range 630–800 nm. The LSPR λ_{max} of this substrate was measured to be 810 nm (12 346 cm^{-1}). The largest SERS enhancement occurs for $\lambda_{ex} = 770$ nm. The maximum of a Gaussian line shape fit to the data is 765 nm (13 072 cm^{-1}). The peak EF value for this sample is 9.3×10^7.

If the peak in the SERS enhancement occurs when the LSPR λ_{max} of the sample is equal to $(\lambda_{ex} + \lambda_{vib})/2$ (where λ_{vib}

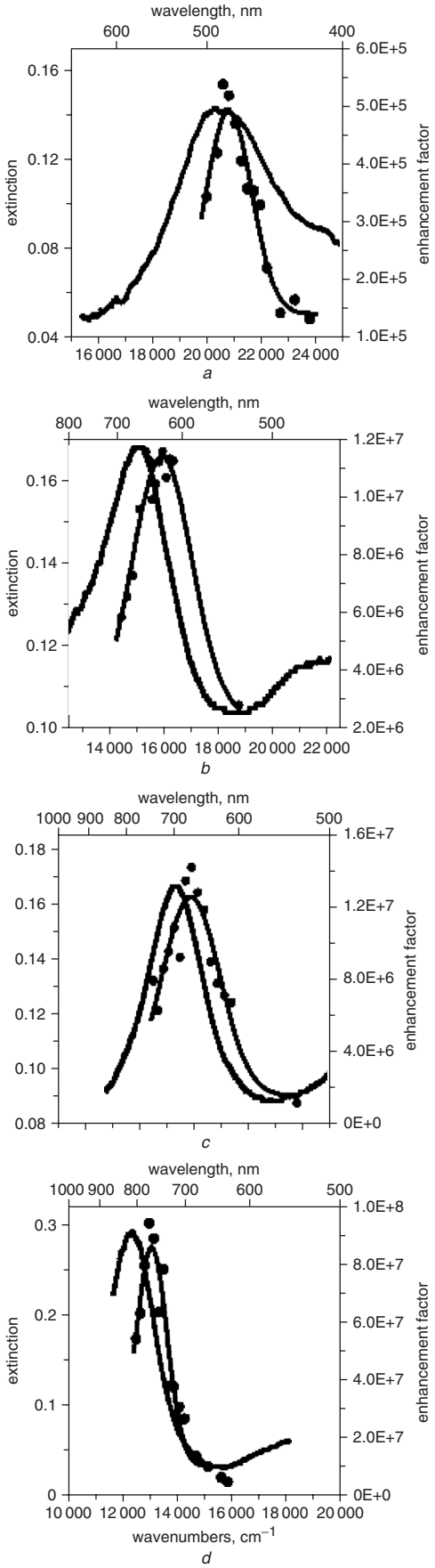

Fig. 4 *Surface-enhanced Raman excitation spectra of 1575 cm^{-1} peak of benzenethiol with cyclohexane as intensity standard*
a Substrate annealed at 300°C for 1 h. LSPR $\lambda_{max} = 489$ nm; profile fit maximum at $\lambda_{ex,max} = 480$ nm
b LSPR $\lambda_{max} = 663$ nm; profile fit maximum at $\lambda_{ex,max} = 625$ nm
c LSPR $\lambda_{max} = 699$ nm; profile fit maximum at $\lambda_{ex,max} = 671$ nm
d LSPR $\lambda_{max} = 810$ nm; profile fit maximum at $\lambda_{ex,max} = 765$ nm

denotes the wavelength of the Raman-shifted peak of interest), then $\lambda_{ex,max}$ should be different for the various Raman bands of benzenethiol on a single sample. It is expected that $\lambda_{ex,max}$ will have a larger separation from the LSPR λ_{max} for a large Raman shift than for a small shift. Excitation spectra for three benzenethiol peaks on a single substrate are shown in Fig. 5. For this substrate, the LSPR λ_{max} is 729 nm. Figure 5*a* shows the SERS excitation profile for the 1575 cm^{-1} peak of benzenethiol, normalised to the 1444 cm^{-1} peak of liquid cyclohexane. The separation in wave numbers between the LSPRs λ_{max} and $\lambda_{ex,max}$ is 734 cm^{-1}. In Fig. 5*b*, the excitation profile for the 1081 cm^{-1} benzenethiol peak (normalised to the 1028 cm^{-1} peak of cyclohexane) is shown. The separation in wave numbers between the LSPRs λ_{max} and $\lambda_{ex,max}$ is 569 cm^{-1}. Finally, in Fig. 5*c*, the excitation profile for the 1009 cm^{-1} benzenethiol peak (normalised to the 1028 cm^{-1} peak of cyclohexane) is shown, and the separation in wave numbers between the LSPR λ_{max} and $\lambda_{ex,max}$ is 488 cm^{-1}.

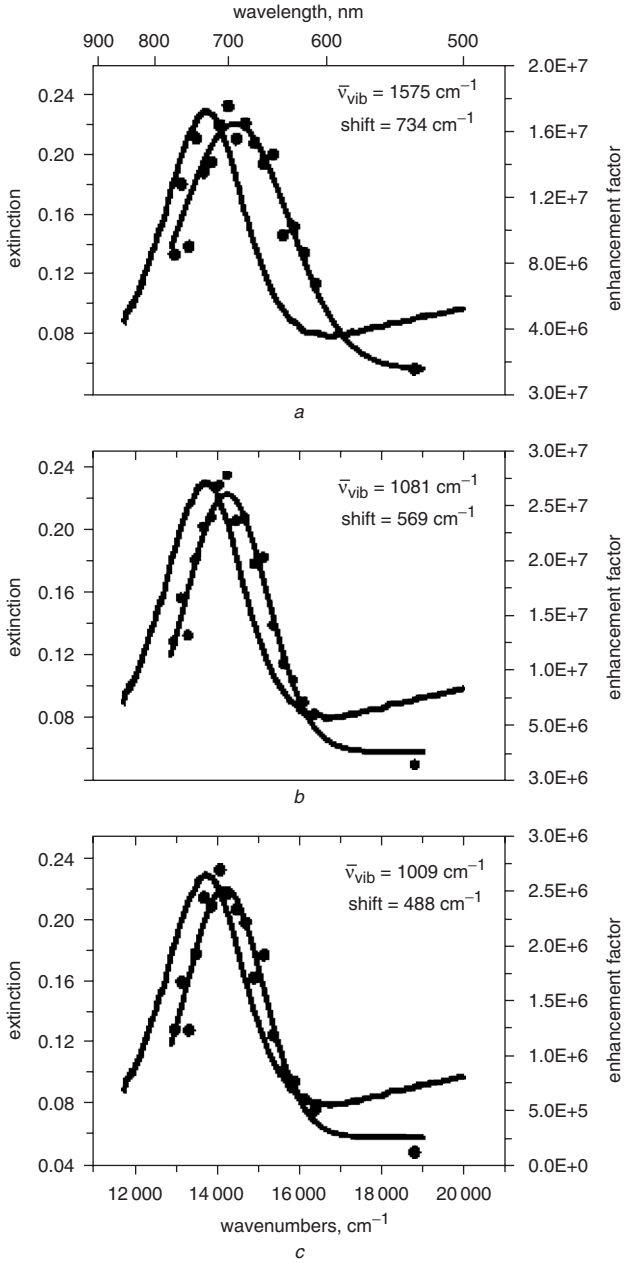

Fig. 5 *Effect of Stokes Raman shift*
a Profile of 1575 cm^{-1} vibration mode of benzenethiol. Distance between LSPR λ_{max} and excitation profile fit line $\lambda_{ex,max}$ = 734 cm^{-1}
b 1081 cm^{-1} vibration mode, shift = 569 cm^{-1}
c 1009 cm^{-1} vibration mode, shift = 488 cm^{-1}

These data demonstrate the qualitative trend whereby the $\lambda_{ex,max}$ in the excitation spectra of larger Raman-shifted bands yield a larger separation from the LSPR λ_{max} than those of smaller Raman-shifted bands. These data lend validation to the EM mechanism as well as highlighting another factor that must be kept in mind in the design of an SERS-based sensor. The relationship between the peak in the SERS enhancement factor and the extinction maximum of the substrate's LSPR has been shown to be dependent upon the magnitude of the Raman shift.

The work above demonstrates the most thorough WS SERES experiments heretofore performed on optically and topographically characterised SERS substrates. The experimental apparatus utilised has been proven effective for the measurement of relative SERS enhancements that vary by three orders of magnitude. This work demonstrates that the relationship between the substrate LSPR and the SERES profile for size-homogenous nanoparticles is consistent throughout the visible range. In all cases, the experimentally observed results are consistent with those predicted by the EM mechanism. Specifically, the maximum SERS enhancement always occurs when the substrate LSPR λ_{max} is located between the laser excitation wavelength, λ_{ex}, and the wavelength of the Raman-scattered photon, λ_{vib}. Under these conditions, both the incident and scattered photons experience strong enhancement by the LSPR. Each substrate exhibits a WS SERES profile that has a similar line shape to the extinction spectrum of the substrate. The largest EF measured was $\sim 10^8$ for the triangular nanoparticle arrays.

Ultimately, refinement of the experimental apparatus and optimisation of SERS enhancement will allow SERES to be performed using single nanoparticle substrates. This level provides the best possible case in terms of reducing sample heterogeneity, in that it will remove the effects of ensemble averaging or particle coupling. These experiments are expected to provide key information to validate the EM mechanism of SERS and will present an additional technique that can be used to study the SMSERS effect.

Our detailed WS SERES studies unequivocally demonstrate the importance of designing SERS experiments such that the LSPR λ_{max} of the substrate is located in between the laser excitation wavelength and the wavelength of the Raman peak of interest. One very attractive feature of the NSL-derived nanoparticle substrates is the tuneability of the LSPR λ_{max} spectral position. Therefore, by using these substrates for SERS-based sensing, we can optimise the sensor by using an excitation wavelength that utilises the ν^4 dependence of Raman scattering while taking into account other factors of the particular application, assembling a detection system that is optimised for highest throughput at the wavelength of interest, and fabricating nanoparticle arrays with an LSPR λ_{max} precisely located in between λ_{ex} and λ_{vib}.

4 Biological applications of surface-enhanced Raman scattering

4.1 Rapid anthrax biomarker detection based on SERS

Anthrax is an infectious disease caused by the spore-forming bacterium *Bacillus anthracis* [78]. Currently, the demand for better field tests for *B. anthracis* spores has increased as a consequence of contaminated mail and false alarms. Several techniques have been developed for real-time detection of *Bacillus* spores [79, 80]. Examples include

fluorescence detection using portable devices, which is sensitive enough to detect $\sim 10^3$ spores in 7 min, but has the potential to give false positive readings [79]. In contrast, SERS possesses highly specific chemical information content and therefore is capable of uniquely identifying target analytes, thereby limiting false positives [2]. We have developed a procedure for the rapid extraction of CaDPA from *B. subtilis* spores (simulants for *B. anthracis* spores), followed by SERS detection on AgFON substrates [21]. These substrates were designed and optimised using the methods described in the preceding sections.

Prior work demonstrates that when the localised surface plasmon resonance maximum of a AgFON substrate closely matches the laser excitation wavelength, the maximum SERS signal intensity results. As AgFONs are not optically transparent, the reflectivity minimum was used to locate the LSPR maximum. AgFON surfaces fabricated using 600 nm spheres show a reflectivity minimum at 753 nm (Fig. 6*a*). In fact, further SERS experiments using AgFON substrates with different polystyrene nanosphere diameters demonstrate that the largest SERS enhancement for 750 nm laser excitation was obtained from the AgFON where $D = 600$ nm [21]. The use of NIR laser light in Raman spectroscopy is advantageous because it causes less photochemical damage to the biological samples and results in much less fluorescence background in the Raman spectrum. Therefore this AgFON substrate was chosen as optimum for the *bacillus* spore detection experiments that follow.

Calcium dipicolinate (CaDPA) was extracted from spores by sonicating in 0.02 M HNO_3 solution for 10 min. Figure 6*b* shows the SERS spectrum of 3.7×10^4 spores in 0.2 µl, 0.02 M HNO_3 on a AgFON substrate ($D = 600$ nm, $dm = 200$ nm), which is dominated by bands associated with CaDPA, in agreement with the previous Raman studies on CaDPA and *bacillus* spores [81–84]. The peak at 1050 cm^{-1} in Fig. 6*b* arises from the symmetrical stretching vibration of NO_3^-. This peak is used as an internal standard to reduce the sample-to-sample deviations, because of its high intensity and spectral isolation.

We show in Fig. 7*a* an LOD of 2550 anthrax spores with a data acquisition period of 1 min and a laser power of 50 mW, well below the level believed to trigger an infection in humans. To put these results into context, previously published SERS studies of *bacillus* spore detection were 200 times less sensitive and required three times more laser power [83]. Recently, Bell and co-workers reported a SERS LOD of ~4 parts per million of dipicolinic acid, *i.e.* 2.4×10^{-5} M, using laser excitation at 532 nm without

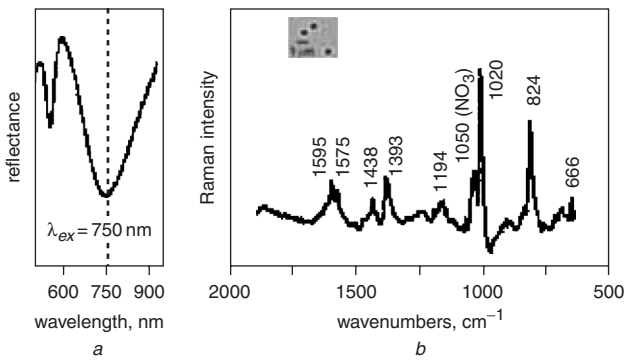

Fig. 6 *Reflectance and SERS spectra*
a UV-vis diffuse reflectance spectrum of AgFON substrate in air
b SERS spectrum of 3.1×10^{-13} M spore suspension (3.7×10^4 spores in 0.2 µl, 0.02 M HNO_3) on AgFON substrate. $\lambda_{ex} = 750$ nm, $P_{ex} = 50$ mW, acquisition time = 1 min, $D = 600$ nm, $d_m = 200$ nm

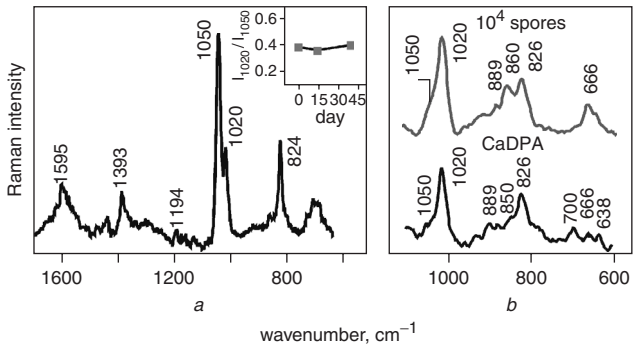

Fig. 7 *SERS spectra*
a SERS spectrum of 2.1×10^{-14} M spore suspension (2.6×10^3 spores in 0.2 µl, 0.02 M HNO_3) on AgFON. Inset shows intensity ratio (I_{1020}/I_{1050}) variation with time. $\lambda_{ex} = 750$ nm, $P_{ex} = 50$ mW, acquisition time = 1 min, $D = 600$ nm, and $d_m = 200$ nm
b SERS spectra obtained by portable Raman spectrometer. Upper spectrum is 8.3×10^{-14} M spore suspension (1.0×10^4 spores in ~0.2 µl, 0.02 M HNO_3) on 30-day-old prefabricated AgFON. Bottom SERS spectrum is 10^{-4} M CaDPA in 0.2 µl 0.02 M HNO_3 on 30-day-old pre-fabricated AgFON substrate. $\lambda_{ex} = 785$ nm, $P_{ex} = 35$ mW, acquisition time = 5 s, resolution = 15 cm^{-1}, $D = 600$ nm, and $d_m = 200$ nm

indicating the laser power [85]. In contrast, the SERS LOD of CaDPA is $\sim 3.1 \times 10^{-6}$ M using the optimised NSL substrate and laser excitation at 750 nm [21]. It should be noted that the intensities of Raman spectra with 750 nm excitation are expected to be about a quarter of those measured with 532 nm excitation, because the Raman signal intensities are inversely proportional to the fourth power of the laser wavelength (see above) [2]. Therefore we calculate an LOD of CaDPA is ~30 times more sensitive than literature values.

Previous research has demonstrated that bare AgFON surfaces display extremely stable SERS activity when challenged by negative potentials in electrochemical experiments [39] and high temperatures in ultrahigh vacuum experiments [86]. In the present example, the intensity ratios between the strongest CaDPA peak at 1020 cm^{-1} and the NO_3^- peak at 1050 cm^{-1} (I_{1020}/I_{1050}) were measured so that prefabricated AgFON substrates of different ages could be compared quantitatively (Fig. 7*a*, inset). The CaDPA intensity remained constant over the course of 40 days, indicating the temporal spectroscopic stability of AgFON substrates over a period of 40 days.

Finally, a portable, handheld SERS device successfully produced a SERS spectrum from 10^4 spores in 5 s using a one-month-old prefabricated AgFON substrate (Fig. 7*a*). The SERS peak positions and intensity pattern for the spore sample were similar to those of CaDPA recorded utilising the same device (Fig. 7*b*). This represents the first reported use of a compact vibration spectrometer for the detection of *bacillus* spores. Coupling the portability and ease of use of this type of device to the molecular specificity and spectral sensitivity inherent in SERS, a range of possibilities become available in the area of detecting bio-agents and other chemical species, such as environmental pollutants, toxic industrial chemicals, process reaction streams, food products etc.

4.2 SERS-based measurement of glucose

Although, the CaDPA biomarker in *Bacillus subtilis* spores directly binds with the silver surface, which is required for SERS detection, many important molecules (e.g. glucose) do not have any natural binding affinity for the silver

surface [37]. Although the normal Raman cross-section of glucose should provide sufficient signal to register on most detection systems [2], the inability to observe glucose using SERS must be attributed to the weak or non-existent interaction of glucose with bare noble metal surfaces. This section demonstrates quantitative glucose detection by tailoring a AgFON substrate similar to that used above with a self-assembled monolayer (SAM) to partition glucose within the range of the enhanced electromagnetic fields on the AgFON surface (Fig. 8) [37], in a manner analogous to that used in high-performance liquid chromatography (HPLC) [87–91]. Functionalising the AgFON substrate with a partition layer has three advantages: the SAM stabilises the Ag surface against oxidation; the SAM is exceedingly stable; and pre-concentration functionality is built in and can be tailored by synthetic control of the partition layer. Such chemical functionalisation of the SERS substrate enables the extension of SERS to previously inaccessible molecules and provides an additional parameter that can be controlled in the development of SERS-based experiments [23].

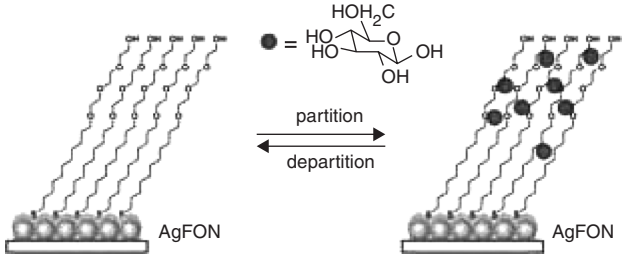

Fig. 8 *Schematic demonstration of hypothetical glucose concentration gradient created by EG3 partition layer*
Alkanethiol portion of EG3 helps form stable SAM, and glycol portion provides hydrophilic environment amenable to glucose salvation

Straight chain alkanethiols and tri(ethylene glycol) terminated alkanethiol (EG3) were found to be effective partition layers. Of the many SAMs tested to determine their effectiveness as a partition layer, EG3 was chosen as a partition layer because of its ability to reject non-specific binding by background proteins [92–95] and its biocompatibility [96, 97], with the goal in mind of progression towards fabrication of an implantable SERS-based glucose sensor. Each EG3-modified AgFON sample was incubated in saline solution with glucose (0–25 mM; 0–450 mg dl^{-1}) at a physiological pH of 7.4. Then, the samples were placed in an environmental control flow cell under saline, and SERS spectra were collected. The spectra were normalised using EG3 peak intensities, followed by partial least squares analysis [36, 37]. The resulting cross-validated glucose concentration predictions are presented in the Clarke error grid (Fig. 10). Clarke and co-workers established the error grid as a metric for evaluating glucose sensor efficacy in the clinically relevant concentration range [98].

The EG3-modified AgFON sensor allows quantitative detection of glucose in the physiological range with a corresponding prediction error of 82 mg dl^{-1} (4.5 mM). In Fig. 9, 94% of the predictions fall in zones A and B, whereas a few data points overlap in zone D within the hypoglycaemic area (< 70 mg dl^{-1}, < 3.9 mM). The error of 82 mg dl^{-1} (4.5 mM) can be partially attributed to slight variation in the EF between different AgFON samples. The nanostructure on a AgFON substrate varies from point to

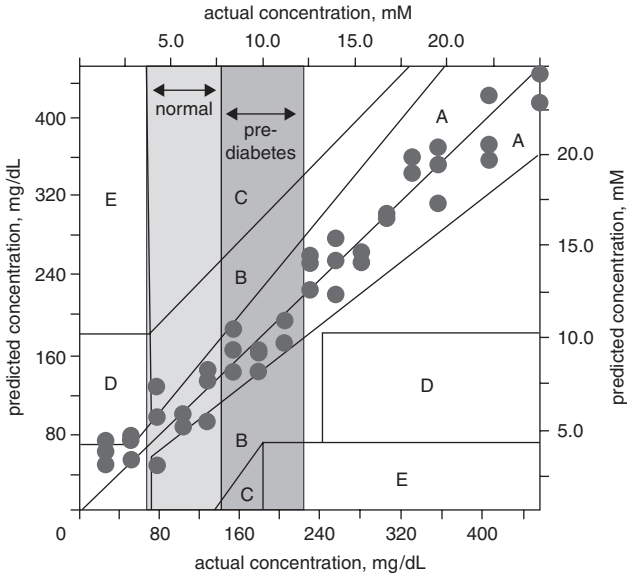

Fig. 9 *Clarke error grid of LOO-PLS predicted glucose concentration against actual glucose concentration (3 loading vectors)*
AgFON samples were fabricated ($D = 390$ nm, $d_m = 200$ nm), incubated for ~16 h in 1 mM EG3 solution, and dosed in glucose solution (range: 0–450 mg/dl, 0–25 mM) for 10 min. Each SERS measurement was made in flow cell under saline with pH = 7.4, using $\lambda_{ex} = 632.8$ nm, $P_{ex} = 1.0$ mW, $t = 30$ s
All SERS measurements were taken in single spot Reproduced with permission from [32]

point, affecting the localised surface plasmon resonance and, accordingly, the EF.

Although quantitative detection is an important characteristic of a viable biosensor, the glucose sensor must also be effective in the presence of interfering proteins. Serum albumin was used to mimic blood serum protein as a challenge to the glucose sensor. The EG3-functionalised AgFON substrate was installed in a flow cell under a saline environment, and the SERS spectrum was obtained (Fig. 10*a*). Then, the BSA solution was injected into the flow cell, and the SERS spectrum was collected throughout the 240 s incubation (Fig. 10*b*). Finally, the sample was exposed to 100 mM glucose, and the SERS spectrum was collected (Fig. 10*c*). Figure 10*d* is the difference spectrum between the sensor under saline and the same surface exposed to the BSA solution, demonstrating that BSA does not have a measurable SERS spectrum on the EG3-modified surface. The lack of SERS bands from BSA is attributed to inefficient adsorption of BSA to the EG3 partition layer. The data in Fig. 10*e* confirm that the SERS glucose sensor is still effective after substrate exposure to an interfering protein and that the peaks correspond to the crystalline glucose peaks shown for comparative reference in Fig. 10*f*. This experiment clearly shows that glucose partitioning into EG3 is not influenced by the presence of large molecules such as serum albumin. It is interesting to note that the peak at 695 cm^{-1} (Fig. 10*a*) shifts to 710 cm^{-1} (Fig. 10*c*) in the presence of glucose. The rearrangement of the SAM when the glucose molecules partition into EG3 may cause this shift. The observed shift in this peak further corroborates the hypothesis of glucose penetrating deeply into the EG3 monolayer, affecting even the character of the C–S bond.

In addition to the demonstration of quantitative glucose measurement in a clinically relevant concentration range and detection of glucose in the presence of other interfering

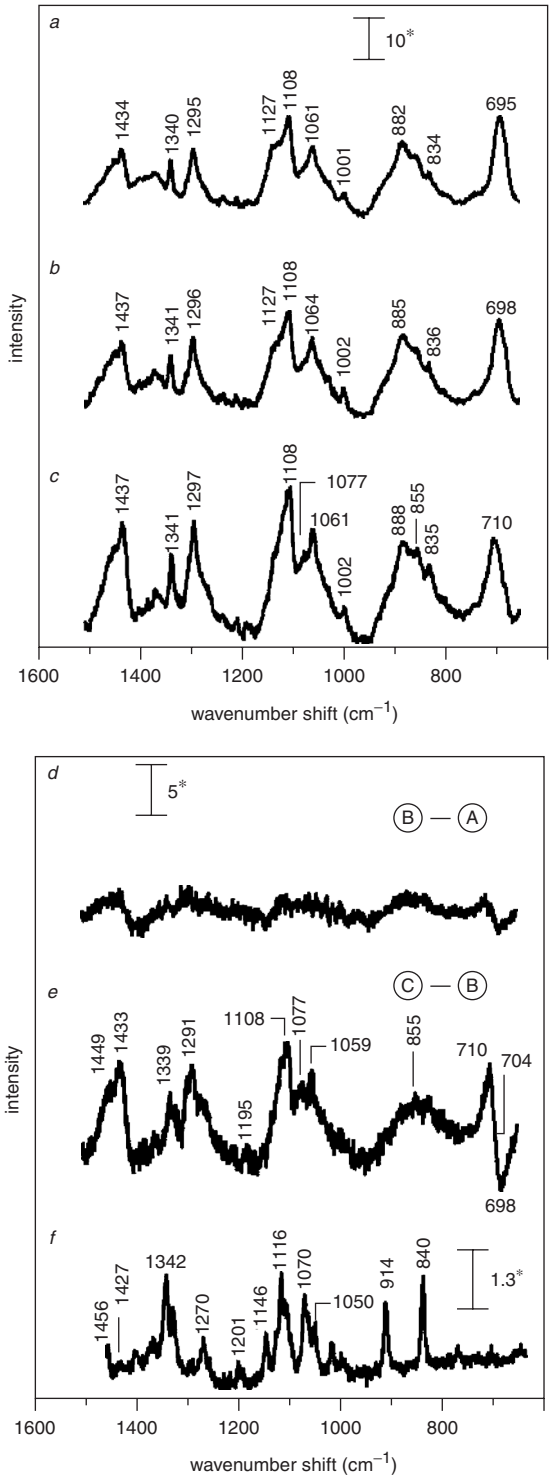

Fig. 10 *SERS spectra showing detection of glucose in presence of serum albumin*

a EG3 monolayer on AgFON substrate, $\lambda_{ex} = 632.8$, $P_{ex} = 0.8$ mW, $t = 240$ s

b 1 mg ml^{-1} serum albumin injected into flow cell to challenge EG3-modified AgFON, $\lambda_{ex} = 632.8$, $P_{laser} = 0.8$ mW, $t = 240$ s

c 100 mM glucose injected into flow cell, $\lambda_{ex} = 632.8$, $P_{ex} = 0.8$ mW, $t = 240$ s

d Difference spectrum obtained by subtracting *a* from *b* revealing lack of SERS spectrum for adsorbed serum albumin

e Difference spectrum obtained by subtracting *b* from *c* indicating serum albumin exposure does not interfere with glucose detection

f Normal Raman spectrum of crystalline glucose for comparison, $\lambda_{ex} = 632.8$, $P_{ex} = 5$ mW, $t = 30$ s $*$ adu mW^{-1} s^{-1}

proteins, other characteristics of the EG3-modified AgFON glucose sensor, such as durability and reusability, are demonstrated in published work [36, 38].

5 Conclusions

SERS is a powerful technique for the sensitive and selective detection of low-concentration analytes. To achieve the lowest limits of detection, both the relationship between surface nanostructure and laser excitation wavelength, as well as the analyte–surface binding chemistry must be carefully optimised. This work exploits the highly tuneable nature of nanoparticle optical properties to establish the first set of optimisation conditions. We conclusively demonstrated that the SERS enhancement factor is optimised when the energy of LSPR lies between the energy of the excitation wavelength and the energy of the vibration band of interest. With the narrow LSPRs used in this work, it is straightforward to achieve an EF of $\sim 10^8$. We also detailed the use of the PS SERES technique to aid in the design of experiments that are unable to exploit a broadly tuneable laser and detector system, i.e. those most routinely available.

The experience garnered in the development of the SERES work was applied to the analytically challenging task of detecting biomarkers for *bacillus* spores. This review also covered the exploitation of chemical modification of SERS substrates to improve the interaction between the surface and target analytes. Specifically, we used the measurement of glucose, a molecule with no detectable SERS signal under normal circumstances, to illustrate how effective surface functionalisation can be for expanding the potential role of SERS.

6 Acknowledgments

The authors gratefully acknowledge the financial support of the Air Force Office of Scientific Research MURI program (F49620-02-1-0381) and the National Science Foundation (DMR-0076097). Any opinions, findings and conclusion or recommendations expressed in this material are those of the authors and do not necessarily reflect those of the National Science Foundation. This project was also supported by the Institute for Bioengineering and Nanoscience in Advanced Medicine at Northwestern University, and the National Institutes of Health (EY13002 and EY13015). The authors wish to acknowledge the following individuals for their experimental assistance, materials or expertise: J.A. Dieringer, L. Chang, M. Glucksberg, C.L. Haynes, E. Jeoung, M. Käll, O. Lyandres, M. Mrksich, C. Murphy, A.D. McFarland, S. Nie, J.C. Riboh, G.C. Schatz, K. Shafer-Peltier, J. Walsh and S. Zou.

7 References

1 Raman, C.V., and Krishnan, K.S.: 'A new type of secondary radiation', *Nature*, 1928, **121**, p. 501

2 McCreery, R.L.: 'Raman spectroscopy for chemical analysis' (John Wiley & Sons, Inc., New York, 2000), p. 420

3 Ashkin, A., and Dziedzic, J.M.: 'Radiation pressure on a free liquid surface', *Phys. Rev. Lett.*, 1973, **30**, pp. 139–142

4 Ashkin, A., Bjorkholm, J.E., and Chu, S.: 'Caught in a trap', *Nature*, 1986, **323**, pp. 585–585

5 Musick, J., Popp, J., Trunk, M., and Kiefer, W.: 'Investigations of radical polymerization and copolymerization reactions in optically levitated microdroplets by simultaneous Raman spectroscopy, MIE scattering, and radiation pressure measurements', *Appl. Spectrosc.*, 1998, **52**, pp. 692–701

6 Ajito, K., Han, C.X., and Torimitsu, K.: 'Detection of glutamate in optically trapped single nerve terminals by Raman spectroscopy', *Anal. Chem.*, 2004, **76**, pp. 2506–2510

7 Haynes, C.L., and Van Duyne, R.P.: 'Plasmon-sampled surface-enhanced Raman excitation spectroscopy', *J. Phys. Chem. B*, 2003, **107**, pp. 7426–7433

8 McFarland, A.D., Young, M.A., Dieringer, J.A., and Van Duyne, R.P.: 'Wavelength-scanned surface-enhanced Raman excitation spectroscopy', *J. Phys. Chem. B*, 2005, **109**, pp. 11279–11285

9 Nie, S., and Emory, S.R.: 'Probing single molecules and single nanoparticles by surface-enhanced Raman scattering', *Science*, 1997, **275**, pp. 1102–1106
10 Kneipp, K., Wang, Y., Kneipp, H., Perelman, L.T., Itzkan, I., Dasari, R.R., and Feld, M.S.: 'Single molecule detection using surface-enhanced Raman scattering', *Phys. Rev. Lett.*, 1997, **78**, pp. 1667–1670
11 Fleischmann, M., Hendra, P.J., and McQuillan, A.J.: 'Raman spectra of pyridine adsorbed at a silver electrode', *Chem. Phys. Lett.*, 1974, **26**, pp. 163–166
12 Schatz, G.C., and Van Duyne, R.P.: 'Electromagnetic mechanism of surface-enhanced spectroscopy' in Chalmers, J.M. and Griffiths, P.R. (Eds.): 'Handbook of vibrational spectroscopy' (Wiley, New York, 2002), Vol. 1, pp. 759–774
13 Jeanmaire, D.L., and Van Duyne, R.P.: 'Surface Raman spectroelectrochemistry. Part I. Heterocyclic, aromatic, and aliphatic amines adsorbed on the anodized silver electrode', *J. Electroanl. Chem. Interfacial Electrochem.*, 1977, **84**, pp. 1–20
14 Albrecht, M.G., and Creighton, J.A.: 'Anomalously intense Raman-spectra of pyridine at a silver electrode', *J. Am. Chem. Soc.*, 1977, **99**, pp. 5215–5217
15 Moskovits, M.: 'Surface-enhanced spectroscopy', *Rev. Mod. Phys.*, 1985, **57**, pp. 783–826
16 Otto, A., Mrozek, I., Grabhorn, H., and Akemann, W.: 'Surface-enhanced Raman scattering', *J. Phys.: Condens. Matter*, 1992, **4**, pp. 1143–1212
17 Otto, A., Mrozek, I., Grabhorn, H., and Akemann, W.: 'Surface-enhanced Raman-scattering', *Journal of Physics-Condensed Matter*, 1992, **4**, pp. 1143–1212
18 Doering, W.E., and Nie, S.M.: 'Single-molecule and single-nanoparticle sers: examining the roles of surface active sites and chemical enhancement', *J. Phys. Chem. B*, 2002, **106**, pp. 311–317
19 Genov, D.A., Sarychev, A.K., Shalaev, V.M., and Wei, A.: 'Resonant field enhancements from metal nanoparticle arrays', *Nano Lett.*, 2004, **4**, pp. 153–158
20 GarciaVidal, F.J., and Pendry, J.B.: 'Collective theory for surface enhanced Raman scattering', *Phys. Rev. Lett.*, 1996, **77**, pp. 1163–1166
21 Zhang, X., Young, M.A., Lyandres, O., and Van Duyne, R.P.: 'Rapid detection of an anthrax biomarker by surface-enhanced Raman spectroscopy', *J. Am. Chem. Soc.*, 2005, **127**, pp. 4484–4489
22 Dick, L.A., Haes, A.J., and Van Duyne, R.P.: 'Distance and orientation dependence of heterogeneous electron transfer: a surface-enhanced resonance Raman scattering study of Cytochrome C bound to carboxylic acid terminated alkanethiols adsorbed on silver electrodes', *J. Phys. Chem. B*, 2000, **104**, pp. 11752–11762
23 Kennedy, B.J., Spaeth, S., Dickey, M., and Carron, K.T.: 'Determination of the distance dependence and experimental effects for modified Sers substrates based on self-assembled monolayers formed using alkanethiols', *J. Phys. Chem. B*, 1999, **103**, pp. 3640–3646
24 Haes, A.J., Zou, S., Schatz, G.C., and Van Duyne, R.P.: 'A nanoscale optical biosensor: the long range distance dependence of the localized surface plasmon resonance of noble metal nanoparticles', *J. Phys. Chem. B*, 2004, **108**, pp. 109–116
25 Cotton, T.M., and Brandt, E.S.: 'Surface-enhanced Raman scattering' in Rossiter, B.W. and Baetzold, R.C. (Eds.): 'Physical methods of chemistry series: investigations of surfaces and interfaces-Part B' (John Wiley & Sons, New York, 1993), Vol. IXB, pp. 633–718
26 Pipino, A.C.R., Van Duyne, R.P., and Schatz, G.C.: 'Surface-enhanced second-harmonic diffraction: experimental investigation of selective enhancement', *Phys. Rev. B: Condens. Matter*, 1996, **53**, pp. 4162–4169
27 Chen, T.T., Vonraben, K.U., Murphy, D.V., Chang, R.K., and Laube, B.L.: 'Surface enhanced Raman-scattering and 2nd-harmonic generation from Cn- complexes and (So4)-S-2- on Ag electrodes during oxidation-reduction cycles', *Surf. Sci.*, 1984, **143**, pp. 369–390
28 Boyd, G.T., Rasing, T., Leite, J.R.R., and Shen, Y.R.: 'Local-field enhancement on rough surfaces of metals, semimetals, and semiconductors with the use of optical 2nd-harmonic generation', *Phys. Rev. B*, 1984, **30**, pp. 519–526
29 Jiang, J., Bosnick, K., Maillard, M., and Brus, L.: 'Single molecule Raman spectroscopy at the junctions of large Ag nanocrystals', *J. Phys. Chem. B*, 2003, **107**, pp. 9964–9972
30 Gunnarsson, L., Bjerneld, E.J., Xu, H., Petronis, S., Kasemo, B., and Kall, M.: 'Interparticle coupling effects in nanofabricated substrates for surface-enhanced Raman scattering', *Appl. Phys. Lett.*, 2001, **78**, pp. 802–804
31 Van Duyne, R.P., Hulteen, J.C., and Treichel, D.A.: 'Atomic force microscopy and surface-enhanced Raman spectroscopy. I. silver island films and silver film over polymer nanosphere surfaces supported on glass', *J. Chem. Phys.*, 1993, **99**, pp. 2101–2115
32 Van Duyne, R.P., Haller, K.L., and Altkorn, R.I.: 'Spatially resolved surface enhanced Raman spectroscopy: feasibility, intensity dependence on sampling area and attomole mass sensitivity', *Chem. Phys. Lett.*, 1986, **126**, pp. 190–196
33 Sun, L.: 'Time-resolved surface enhanced Raman scattering studies of substrate morphology transformation and surface adsorption/desorption kinetics at colloidal and electrochemical interfaces'. Thesis, 1990, Northwestern University, Evanston, IL 60208
34 Bokor, J.: 'Ultrafast dynamics at semiconductor and metal-surfaces', *Science*, 1989, **246**, pp. 1130–1134
35 Hofer, U., Shumay, I.L., Reuss, C., Thomann, U., Wallauer, W., and Fauster, T.: 'Time-resolved coherent photoelectron spectroscopy of quantized electronic states on metal surfaces', *Science*, 1997, **277**, pp. 1480–1482
36 Yonzon, C.R., Haynes, C.L., Zhang, X., Walsh, J.T. Jr., and Van Duyne, R.P.: 'A glucose biosensor based on surface-enhanced Raman scattering: improved partition layer, temporal stability, reversibility, and resistance to serum protein interference', *Anal. Chem.*, 2004, **76**, pp. 78–85
37 Shafer-Peltier, K.E., Haynes, C.L., Glucksberg, M.R., and Van Duyne, R.P.: 'Toward a glucose biosensor based on surface-enhanced Raman scattering', *J. Am. Chem. Soc.*, 2003, **125**, pp. 588–593
38 Stuart, D.A., Yonzon, C.R., Zhang, X., Lyandres, O., Shah, N., Glucksberg, M.R., Walsh, J.Y., and Van Duyne, R.P.: 'Glucose sensing using near infrared surface-enhanced Raman spectroscopy: gold surfaces, 10-day stability, and improved accuracy', *Anal. Chem.*, 2005, (In press)
39 Zhang, X., Yonzon, C.R., and Van Duyne, R.P.: 'An electrochemical surface-enhanced Raman spectroscopy approach to anthrax detection', *Proc. SPIE-Int. Soc. Opt. Eng.*, 2003, **5221**, pp. 82–91
40 Grabar, K.C., Freeman, R.G., Hommer, M.B., and Natan, M.J.: 'Preparation and characterization of Au colloid monolayers', *Anal. Chem.*, 1995, **67**, pp. 735–743
41 Allen, C.S., and Van Duyne, R.P.: 'Molecular generality of surface-enhanced Raman spectroscopy. A detailed investigation of the hexacyanoruthenate ion adsorbed on silver and copper electrodes', *J. Am. Chem. Soc.*, 1981, **103**, pp. 7497–7501
42 Kreibig, U., Gartz, M., Hilger, A., and Hovel, H.: 'Optical investigations of surfaces and interfaces of metal clusters' in Duncan, M.A. (Ed.): 'Advances in metal and semiconductor clusters' (JAI Press Inc., Stamford, 1998), Vol. 4, pp. 345–393
43 Volkan, M., Stokes, D.L., and Vo-Dinh, T.: 'A new surface-enhanced Raman scattering substrate based on silver nanoparticles in sol-gel', *J. Raman Spectrosc.*, 1999, **30**, pp. 1057–1065
44 Zeisel, D., Deckert, V., Zenobi, R., and Vo-Dinh, T.: 'Near-field surface-enhanced Raman spectroscopy of dye molecules adsorbed on silver island films', *Chem. Phys. Lett.*, 1998, **283**, pp. 381–385
45 Dick, L.A., McFarland, A.D., Haynes, C.L., and Van Duyne, R.P.: 'Metal film over nanosphere (Mfon) electrodes for surface-enhanced Raman spectroscopy (Sers): improvements in surface nanostructure stability and suppression of irreversible loss', *J. Phys. Chem. B*, 2002, **106**, pp. 853–860
46 El-Sayed, M.A.: 'Some interesting properties of metals confined in time and nanometer space of different shapes', *Accounts of Chemical Research*, 2001, **34**, pp. 257–264
47 Xia, Y., Halas, N.J., and Editors, G.: 'Shape-controlled synthesis and surface plasmonic properties of metallic nanostructures', *MRS Bulletin*, 2005, **30**, pp. 338–348
48 Wiley, B., Sun, Y., Chen, Y., Cang, H., Li, Z.-Y., Li, X., and Xia, Y.: 'Shape-controlled synthesis of silver and gold nanostructures', *MRS Bulletin*, 2005, **30**, pp. 356–361
49 Kottmann, J.P., Martin, O.J.F., Smith, D.R., and Schultz, S.: 'Dramatic localized electromagnetic enhancement in plasmon resonant nanowires', *Chem. Phys. Lett.*, 2001, **341**, pp. 1–6
50 Tao, A., Kim, F., Hess, C., Goldberger, J., He, R.R., Sun, Y.G., Xia, Y.N., and Yang, P.D.: 'Langmuir-Blodgett silver nanowire monolayers for molecular sensing using surface-enhanced Raman spectroscopy', *Nano Lett.*, 2003, **3**, pp. 1229–1233
51 Caldwell, W.B., Campbell, D.J., Chen, K.M., Herr, B.R., Mirkin, C.A., Malik, A., Durbin, M.K., Dutta, P., and Huang, K.G.: 'A highly ordered self-assembled monolayer film of an azobenzene-alkanethiol on Au(111) - electrochemical properties and structural characterization by synchrotron in-plane X-ray-diffraction, atomic-force microscopy, and surface-enhanced Raman-spectroscopy', *J. Am. Chem. Soc.*, 1995, **117**, pp. 6071–6082
52 Caldwell, W.B., Chen, K.M., Herr, B.R., Mirkin, C.A., Hulteen, J.C., and Vanduyne, R.P.: 'Self-assembled monolayers of ferrocenylazobenzenes on Au(111)/mica films - surface-enhanced Raman-scattering response vs surface-morphology', *Langmuir*, 1994, **10**, pp. 4109–4115
53 Xu, S.P., Zhao, B., Xu, W.Q., and Fan, Y.G.: 'Preparation of Au-Ag coreshell nanoparticles and application of bimetallic sandwich in surface-enhanced Raman scattering (Sers)', *Colloids and Surfaces a-Physicochemical and Engineering Aspects*, 2005, **257-58**, pp. 313–317
54 Doering, W.E., and Nie, S.M.: 'Spectroscopic tags using dye-embedded nanoparticies and surface-enhanced Raman scattering', *Anal. Chem.*, 2003, **75**, pp. 6171–6176
55 Muniz-Miranda, M., and Ottaviani, M.F.: 'Silver nanoclusters in mesoporous silica, as obtained by visible-laser irradiation', *Laser Phys.*, 2004, **14**, pp. 1533–1538
56 Kneipp, K., Haka, A.S., Kneipp, H., Badizadegan, K., Yoshizawa, N., Boone, C., Shafer-Peltier, K.E., Motz, J.T., Dasari, R.R., and Feld, M.S.: 'Surface-enhanced Raman spectroscopy in single living cells using gold nanoparticles', *Appl. Spectrosc.*, 2002, **56**, pp. 150–154
57 Thygesen, L.G., Jorgensen, K., Moller, B.L., and Engelsen, S.B.: 'Raman spectroscopic analysis of cyanogenic glucosides in plants: development of a flow injection surface-enhanced Raman scatter (Fi-Sers) method for determination of cyanide', *Appl. Spectrosc.*, 2004, **58**, pp. 212–217
58 Felidj, N., Aubard, J., Levi, G., Krenn, J. R., Salerno, M., Schider, G., Lamprecht, B., Leitner, A., and Aussenegg, F.R.: 'Controlling the optical response of regular arrays of gold particles for surface-enhanced Raman scattering', *Physical Review B, Condensed Matter and Materials Physics*, 2002, **65**, pp. 075419/075411–075419/075419
59 Kahl, M., Voges, E., Kostrewa, S., Viets, C., and Hill, W.: 'Periodically structured metallic substrates for Sers', *Sensors and Actuators B*, 1998, **51**, pp. 285–291

60 Hulteen, J.C., and Van Duyne, R.P.: 'Nanosphere lithography: a materials general fabrication process for periodic particle array surfaces', *J. Vacuum Sci. Tech. A*, 1995, **13**, pp. 1553–1558
61 Hulteen, J.C., Treichel, D.A., Smith, M.T., Duval, M.L., Jensen, T.R., and Van Duyne, R.P.: 'Nanosphere lithography: size-tunable silver nanoparticle and surface cluster arrays', *J. Phys. Chem. B*, 1999, **103**, pp. 3854–3863
62 Dimitrov, A.S., and Nagayama, K.: 'Continuous convective assembling of fine particles into two-dimensional arrays on solid surfaces', *Langmuir*, 1996, **12**, pp. 1303–1311
63 Dimitrov, A.S., Miwa, T., and Nagayama, K.: 'A comparison between the optical properties of amorphous and crystalline monolayers of silica particles', *Langmuir*, 1999, **15**, pp. 5257–5264
64 Litorja, M., Haynes, C.L., Haes, A.J., Jensen, T.R., and Van Duyne, R.P.: 'Surface-enhanced Raman scattering detected temperature programmed desorption: optical properties, nanostructure, and stability of silver film over Sio2 nanosphere surfaces', *J. Phys. Chem. B*, 2001, **105**, pp. 6907–6915
65 Haynes, C.L., and Van Duyne, R.P.: 'Plasmon-sampled surface-enhanced raman excitation spectroscopy', *J. Phys. Chem. B*, 2003, **107**, pp. 7426–7433
66 Jensen, T.R., Malinsky, M.D., Haynes, C.L., and Van Duyne, R.P.: 'Nanosphere lithography: tunable localized surface plasmon resonance spectra of silver nanoparticles', *J. Phys. Chem. B*, 2000, **104**, pp. 10549–10556
67 Haynes, C.L., and Van Duyne, R.P.: 'Nanosphere lithography: a versatile nanofabrication tool for studies of size-dependent nanoparticle optics', *J. Phys. Chem. B*, 2001, **105**, pp. 5599–5611
68 Blatchford, C.G., Campbell, J.R., and Creighton, J.A.: 'Plasma resonance - enhanced raman scattering by adsorbates on gold colloids: the effects of aggregation', *Surf. Sci.*, 1982, **120**, pp. 435–455
69 Vlckova, B., Gu, X.J., and Moskovits, M.: 'Sers excitation profiles of phthalazine adsorbed on single colloidal silver aggregates as a function of cluster size', *J. Phys. Chem. B*, 1997, **101**, pp. 1588–1593
70 Gregory, B.W., Clark, B.K., Standard, J.M., and Avila, A.: 'Localization of image state electrons in the sulfur headgroup region of alkanethiol self-assembled films', *J. Phys. Chem. B*, 2001, **105**, pp. 4684–4689
71 Von Raben, K.U., Chang, R.K., Laube, B.L., and Barber, P.W.: 'Wavelength dependence of surface-enhanced raman scattering from silver colloids with adsorbed cyanide complexes, sulfite and pyridine', *J. Phys. Chem.*, 1984, **88**, pp. 5290–5296
72 Weitz, D.A., Garoff, S., and Gramila, T.J.: 'Excitation spectra of surface-enhanced raman scattering on silver-island films', *Optics Lett.*, 1982, **7**, pp. 168–170
73 Kerker, M., Siiman, O., and Wang, D.S.: 'Effect of aggregates on extinction and surface-enhanced raman scattering spectra of colloidal silver', *J. Phys. Chem.*, 1984, **88**, pp. 3168–3170
74 Fornasiero, D., and Grieser, F.: 'Analysis of the visible absorption and sers excitation spectra of silver sols', *J. Chem. Phys.*, 1987, **87**, pp. 3213–3217
75 Feilchenfeld, H., and Siiman, O.: 'Surface raman excitation and enhancement profiles for chromate, molybdate, and tungstate on colloidal silver', *J. Phys. Chem.*, 1986, **90**, pp. 2163–2168
76 Liao, P.F., Bergman, J.G., Chemla, D.S., Wokaun, A., Melngailis, J., Hawryluk, A.M., and Economou, N.P.: 'Surface-enhanced Raman scattering from microlithographic silver particle surfaces', *Chem. Phys. Lett.*, 1981, **82**, pp. 355–359
77 Felidj, N., Aubard, J., Levi, G., Krenn, J.R., Hohenau, A., Schider, G., Leitner, A., and Aussenegg, F.R.: 'Optimized surface-enhanced raman scattering on gold nanoparticle arrays', *Appl. Phys. Lett.*, 2003, **82**, pp. 3095–3097
78 Walt, D.R., and Franz, D.R.: 'Biological warfare detection', *Anal. Chem.*, 2000, **72**, pp. 738A–746A
79 Pellegrino, P.M., Fell, N.F., and Gillespie, J.B.: 'Enhanced spore detection using dipicolinate extraction techniques', *Analytica Chimica Acta*, 2002, **455**, p. 167
80 Ryu, C., Lee, K., Yoo, C., Seong, W.K., and Oh, H.: 'Sensitive and rapid quantitative detection of anthrax spores isolated from soil samples by real-time pcr', *Microbiol. Immunol.*, 2003, **47**, pp. 693–699
81 Woodruff, W.H., Spiro, T.G., and Gilvarg, C.: 'Raman-spectroscopy invivo - evidence on structure of dipicolinate in intact spores of Bacillus-Megaterium', *Biochem. Biophys. Res. Commun.*, 1974, **58**, pp. 197–203
82 Carmona, P.: 'Vibrational spectra and structure of crystalline dipicolinic acid and calcium dipicolinate trihydrate', *Spectrochim. Acta, Part A*, 1980, **36A**, pp. 705–712
83 Farquharson, S., Grigely, L., Khitrov, V., Smith, W., Sperry, J.F., and Fenerty, G.: 'Detecting bacillus cereus spores on a mail sorting system using raman spectroscopy', *J. Raman Spectrosc.*, 2004, **35**, pp. 82–86
84 Chan, J.W., Esposito, A.P., Talley, C.E., Hollars, C.W., Lane, S.M., and Huser, T.: 'Reagentless identification of single bacterial spores in aqueous solution by confocal laser tweezers raman spectroscopy', *Anal. Chem.*, 2004, **76**, pp. 599–603
85 Bell, S.E.J., Mackle, J.N., and Sirimuthu, N.M.S.: 'Quantitative surface-enhanced Raman spectroscopy of dipicolinic acid - towards rapid anthrax endospore detection', *Analyst*, 2005, **130**, pp. 545–549
86 Litorja, M., Haynes, C.L., Haes, A.J., Jensen, T.R., and Van Duyne, R.P.: 'Surface-enhanced Raman scattering detected temperature programmed desorption: optical properties, nanostructure, and stability of silver films over Sio_2 nanospheres', *J. Phys. Chem. B*, 2001, **105**, pp. 6907–6915
87 Blanco Gomis, D., Muro Tamayo, J., and Alonso., M.: 'Determination of monosaccharides in cider by reversed-phase liquid chromatography', *Anal. Chim. Acta*, 2001, **436**, p. 173
88 Carron, K.T., and Kennedy, B.J.: 'Molecular-specific chromatographic detector using modified sers substrates', *Anal. Chem.*, 1995, **67**, pp. 3353–3356
89 Yang, L., Janle, E., Huang, T., Gitzen, J., Kissinger, P.T., Vreeke, M., and Heller, A.: 'Applications of "Wired" peroxidase electrodes for peroxide determination in liquid chromatography coupled to oxidase immobilized enzyme reactors', *Anal. Chem.*, 1995, **34**, pp. 1326–1331
90 Deschaines, T.O., and Carron, K.T.: 'Stability and surface uniformity of selected thiol-coated sers surfaces', *Appl. Spectrosc.*, 1997, **51**, pp. 1355–1359
91 Freunscht, P., Van Duyne, R.P., and Schneider, S.: 'Surface-Enhanced raman spectroscopy of *trans*-stilbene adsorbed on silver film over nanosphere surfaces modified by platinum or alkanethiol deposition', *Chem. Phys. Lett.*, 1997, **281**, pp. 372–378
92 Ostuni, E., Chapman, R.G., Liang, M.N., Meluleni, G., Pier, G., Ingber, D.E., and Whitesides, G.M.: 'Self-assembled monolayers that resist the adsorption of proteins and the adhesion of bacterial and mammalian cells', *Langmuir*, 2001, **17**, pp. 6336–6343
93 Lahiri, J., Isaacs, L., Tien, J., and Whitesides, G.M.: 'A strategy for the generation of surfaces presenting ligands for studies of binding based on an active ester as a common reactive intermediate: a surface plasmon resonance study', *Anal. Chem.*, 1999, **71**, pp. 777–790
94 Clark, S.L., and Hammond, P.T.: 'Engineering the microfabrication of layer-by-layer thin films', *Adv. Mater.*, 1998, **10**, pp. 1515–1519
95 Prime, K.L., and Whitesides, G.M.: 'Adsorption of proteins onto surfaces containing end-attached oligo(ethylene oxide) – a model system using self-assembled monolayers', *J. Am. Chem. Soc.*, 1993, **115**, pp. 10714–10721
96 Lee, J. H., Kopecek, J., and Andrade, J.D.: 'Protein-resistant surfaces prepared by peo-containing block copolymer surfactants', *J. Biomed. Mater. Res.*, 1989, **23**, pp. 351–368
97 Mauzac, M.A.N., and Jozefonvicz, J.: 'Antithrombic activity of some polysaccharide resins', *Biomaterials*, 1982, **3**, pp. 221–224
98 Clarke, W.L., Cox, D., Gonder-Frederick, L.A., Carter, W., and Pohl, S.L.: 'Evaluating clinical accuracy of systems for self-monitoring of blood glucose', *Diabetes Care*, 1987, **10**, pp. 622–628